

## Advection of finite-size particles in open flows

Izabella Julia Benczik,<sup>1</sup> Zoltán Toroczkai,<sup>2</sup> and Tamás Tél<sup>1</sup>

<sup>1</sup>*Institute for Theoretical Physics, Eötvös University, P. O. Box 32, H-1518 Budapest, Hungary*

<sup>2</sup>*Theoretical Division, Los Alamos National Laboratory, Los Alamos, New Mexico 87545*

(Received 4 August 2002; revised manuscript received 28 October 2002; published 21 March 2003)

It is known that small, spherical particles with inertia do not follow the local velocity field of the flow. Here we investigate the motion of such particles and particle ensembles immersed in open, unsteady flows which, in the case of ideal pointlike tracers, generate chaotic Lagrangian trajectories. Due to the extra force terms in the equations of motion (such as Stokes drag, added mass) the inertial tracer trajectories become described by a high-dimensional ( $2d+1$ , with  $d$  being the flow's dimension) chaotic dynamics, which can drastically differ from the  $(d+1)$ -dimensional ideal tracer dynamics. As a consequence, we find parameter regimes (in terms of density and size), where long-term tracer trapping can occur for the inertial particle, even for flows in which no ideal, pointlike passive tracers can be trapped. These studies are performed in a model of a two-dimensional channel flow past a cylindrical obstacle. Since the Lagrangian tracer dynamics is sensitive to the particle density and size parameters, a simple geometric setup in such flows could be used as a (low-density) particle mixture segregator.

DOI: 10.1103/PhysRevE.67.036303

PACS number(s): 47.52.+j, 07.07.Df, 05.45.Jn, 47.55.Kf

### I. INTRODUCTION

Recently, there has been an increasing interest in chaotic advection [1–3] and its applications. In many situations it is important to take into account that the advected particles are of *finite size* and can be *heavier or lighter* than the fluid. Therefore, such particles will follow the fluid motion with some *inertia* only [4–21]. This means that they have the tendency to take over the velocity of the surrounding fluid due to viscosity (Stokes drag), and will do so if the fluid velocity does not change at all, or if it changes very slowly. In the general case, however, the fluid has changed its velocity by the time the particle could have approached it. This effect alone can be a source of chaotic behavior [22].

Understanding the dynamics of inertial particles and ensembles is of paramount importance for many practical applications, ranging from geophysical sciences (such as pollutant transport, cloud formation, motion of balloons or buoys) to industrial applications [13,9,11]. Many practical studies target the modeling of aerosol and pollutant transport, using large scale simulations. The majority of simulations models the particle transport as if it were a passive, massless, pointlike (ideal) tracer, which simply follows the flow. This approximation, as we show, can lead to rather severe errors, of order one, in computing tracer trajectories or ensemble dynamics.

The paper is organized as follows. In Sec. II we briefly recall the equation of motion for advected particles if they are of finite size and have small inertia. In Sec. III we define the analytical model flow used in this paper, which is an open flow in the wake of a solid cylinder where the von Kármán vortex street is located. Section IV discusses the form of the inertial particle trajectories in comparison with the passive ones. The principal characteristics of the ensemble dynamics are treated in Sec. V: the escape rates (*A*), the residence time statistics (*B*), and the invariant sets with fractal properties at different time scales (*C*). We point out the possibility for light particles of having attractors in the

inertial dynamics, even in open flows. In Sec. VI we study the nature of these attractors. In Sec. VII we present how a simple geometrical setup can be used as a particle mixture segregator. Next we demonstrate with a simple calculation that the phenomenon of trapping is a generic property resulting from the nonlinear interaction of the temporal dependence of the underlying flow and the size and inertia effects. The last section contains concluding remarks.

### II. THE EQUATION OF MOTION

The total force exerted on a small spherical particle of radius  $a$  and mass  $m_p$  immersed in a fluid is given by

$$F_i = m_p g_i + \oint \sigma_{ij} n_j dS, \quad i = 1, \dots, d, \quad (1)$$

where  $\mathbf{g}$  is the gravitational acceleration (and creates the buoyancy force),  $\sigma_{ij}$  is the fluid stress tensor on the sphere and the integration is over the surface of the sphere. Here  $d$  is the dimensionality of the flow, typically  $d=2$  or  $d=3$ . In this paper we concentrate on two-dimensional ( $d=2$ ) flows, and assume that the buoyancy force is nonexistent. The presence of the particle in the fluid adds a no-slip boundary condition to the time-dependent Navier-Stokes equation modifying the flow locally. The stress tensor can be approximately evaluated to yield the most important force terms in the equation of motion for the particle [5–13]

$$F_i = m_f \frac{du_i}{dt} - \frac{m_f}{2} \left( \frac{dv_i}{dt} - \frac{du_i}{dt} \right) - 6\pi a \mu (v_i - u_i), \quad (2)$$

where the terms from left to right are as follows.

(1) The fluid force on the particle from the undisturbed flow field  $\mathbf{u}$ , and  $d/dt$  is the total derivative following the fluid motion, i.e.,

$$\frac{du_i}{dt} = \frac{\partial u_i}{\partial t} + (\mathbf{u} \cdot \nabla) u_i. \quad (3)$$

(2) The added mass term, expressing the fact that an inertial particle brings into motion a certain amount of fluid, too, proportional to half of its volume, where  $m_f$  is the mass of the displaced fluid (here we use the corrected version as derived by Auton *et al.* [7]).

(3) The Stokes drag, proportional to the difference between  $v_i$ , the particle velocity and  $u_i$ , the flow velocity, and vanishing for pointlike tracers. An additional force contribution is the Boussinesq-Basset history integral term  $-6\pi a^2 \mu \int_0^t d\tau \{ [d(v_i - u_i)]/d\tau \} / \sqrt{\pi \nu (t - \tau)}$ , where  $\mu$  and  $\nu$  are the fluid's dynamic and kinematic viscosities, respectively. The history term represents the effects of the diffusion of vorticity around the spherical particle, but in many cases it can be dropped from the equations. For a list of conditions where this cannot be neglected, see Ref. [13]. In the following we will drop from our calculations the history term which in the parameter region studied by us is justified [13]. We assume that the particles are so small, and their concentration so low, that they do not modify the flow field or interact with each other. A first step towards the description of cases with large particle concentration could be the investigation of excluded volume effects and the inclusion of local velocity fields, Stokeslets, generated by each moving particle [23], which we leave for further studies.

Thus, based on Eq. (2), the equations of motion  $F_i = m_p dv_i/dt$  for an inertial tracer can be cast in the dimensionless form [20]:

$$\frac{d\mathbf{v}}{dt} - \frac{3}{2}R \frac{d\mathbf{u}}{dt} = -A(\mathbf{v} - \mathbf{u}). \quad (4)$$

The two parameters are the ‘‘mass ratio parameter’’  $R$  and the ‘‘inertia or size parameter’’  $A$  given by

$$R = \frac{2\rho_f}{\rho_f + 2\rho_p}, \quad (5)$$

$$A = R/St, \quad St = \frac{2}{9} \left( \frac{a}{L} \right)^2 \text{Re}, \quad (6)$$

where  $\rho_f$  and  $\rho_p$  are the densities of the fluid and the particle,  $St$  is the particle Stokes number (or the dimensionless decay time due to the Stokes drag),  $\text{Re} = UL/\nu$  is the fluid Reynolds number,  $L$  is a typical large-scale mixing length and  $U$  is a typical large-scale fluid velocity. The tracer equation (4) is valid only for initial tracer velocities matching the fluid velocity [5].

The presence of the coefficient  $3R/2$  expresses the added mass effect, which is not present for neutrally buoyant particles, where  $R = 2/3$ . If  $0 < R < 2/3$ , the particle is heavier than the fluid. This is called the *aerosol* range [6]. For  $2/3 < R < 2$  the particle is lighter than the surrounding fluid. This is called the *bubble* range [6].

The limit  $A \rightarrow \infty$  (irrespective of  $R$ ) corresponds to the passive ideal tracer limit. As we shall see, the most relevant parameter responsible for tracer and fluid trajectory devia-

tions is the inertia parameter  $A$ . The smaller  $A$ , the more pronounced is the effect. This effect can be of order one even for very small particles in a flow with chaotic Lagrangian dynamics [19,22], or in turbulent flows [16].

For nonturbulent, low Reynolds number ( $\text{Re}$ ) flows, with  $\text{Re}$  on the order of hundreds, the particle dynamics is typically *chaotic* [1–3]. Therefore, small deviations between particle trajectories will grow exponentially in time at a rate given by the largest positive Lyapunov exponent.

From Eq. (4) it follows that the inertial dynamics is dissipative. In incompressible flows, to which we restrict ourselves, the phase space contraction rate is  $dA$ , positive in contrast to the ideal case which is area preserving. This opens the possibility of having attractors in the dynamics.

The general inertial dynamics (4) possesses a high-dimensional phase space. For advection in planar flows, besides the two coordinates  $(x, y)$ , two velocity components  $(v_x, v_y)$  should also be taken into account. Since the flow we shall consider is time dependent, periodic, the phase space is five dimensional. On stroboscopic snapshots, a four-dimensional map with variables  $(x, y, v_x, v_y)$  governs the dynamics. It is to be noted that attractors or any other invariant sets exist in the full phase space, but what we observe in the plane of the flow is always a *projection* of these sets on the configuration space. The mere position of the particle does not contain information on the tracer velocity, which is in general different from that of the flow.

### III. THE OPEN FLOW MODEL

In this paper, we show that the inclusion of inertia and size parameters of a small spherical particle as shown in Eq. (4), can lead to drastic changes in the chaotic advection dynamics of the inertial tracer even in open flows [20]. In particular we are interested in the behavior of finite-size tracers in the wake of obstacles (such as a stick, a pillar or an island) for low- $\text{Re}$  flows, where the Eulerian velocity is smooth in space and periodic in time. Ideal tracers are known to exhibit in such time-periodic open flows transient chaos [24]: they can stay in the wake over finite times, but ultimately all the particles escape. This behavior is in contrast with the everyday observation according to which light particles or objects, like e.g., empty coke cans, can be trapped in the wake for arbitrarily long times. This will be explained by the finite-size effects described by Eq. (4).

As a workbench system, we consider a model of the von Kármán vortex street in the wake of a cylinder [24]. Due to the incompressibility of the flow, we can define a streamfunction  $\Psi = \Psi(x, y, t)$  such that

$$u_x = \frac{\partial \Psi}{\partial y}, \quad u_y = -\frac{\partial \Psi}{\partial x}. \quad (7)$$

By measuring the length in units of the cylinder radius, which is simultaneously the characteristic linear size  $L$  of the flow, and taking the period  $T$  of the flow as the time unit, the dimensionless model streamfunction is given by the product:  $\Psi = fg$ , where

$$f(x,y) = 1 - e^{-(\sqrt{x^2+y^2}-1)^2} \quad (8)$$

ensures the presence of a boundary layer (fluid velocity disappearing along the unit circle, which is the surface of the cylinder), and

$$g = -wh_1g_1 + wh_2g_2 + u_0ys \quad (9)$$

describes the periodic detachment of vortices. Here  $w$  represents the average strength of the vortices, and

$$h_1(t) = \sin^2(\pi t), \quad h_2(t) = \cos^2(\pi t), \quad (10)$$

are functions characterizing the time evolution of the vorticity. In Eq. (9)  $u_0$  is the dimensionless background velocity, and  $s = s(x,y) = 1 - \exp[-(x-1)^2/c^2 - (y)^2]$  is a shielding factor, which suppresses the background velocity in the wake. The factors

$$g_i(x,y,t) = e^{-r_0[(x-x_i)^2 + c^2(y+(-1)^i y_0)^2]}, \quad i=1,2 \quad (11)$$

describe the Gaussian forms of the vortices of dimensionless size  $1/\sqrt{r_0}$ , whose positions in the wake are  $x_1(t), y_0$  and  $x_2(t), -y_0$ , respectively, with  $x_1(t) = 1 + l\{t\}, x_2(t) = x_1(t) - 1/2$ , where  $l$  is the dimensionless distance a vortex passes during its lifetime, and  $0 \leq \{z\} < 1$  denotes the fractional part of  $z$ . The parameters held fixed in this paper are  $u_0 = 14$ ,  $r_0 = 0.35$ ,  $y_0 = 0.3$ ,  $c = 2$ , and  $l = 2$ . The same model with  $h_1 = |\sin(\pi t)|$ ,  $h_2 = |\cos(\pi t)|$ ,  $w = 24$  has been checked to be consistent with the passive advection in a Navier-Stokes simulation at fluid Reynolds number about 250 [24]. Since the dynamics of inertial tracers contains the temporal derivative of the velocity, we are replacing the original forms of  $h_1, h_2$  by the smoother terms given by Eq. (10). In order to produce the same qualitative behavior, we have to consider a flow with larger values of  $w$  than in Ref. [24] so that the vortex strength averaged over time units stays the same. In the following we present the numerical results either for the enlarged value  $w = 192/\pi$  or for  $w = 24$ .

#### IV. SAMPLE TRAJECTORIES

In this section we demonstrate pictorially how, due to the finite-size effects, the inertial tracer's trajectories deviate from the passive ones and how their complicated shapes approach the Hamiltonian limit, as  $A$  increases. We present the results of a few runs to compare inertial tracer trajectories with the same initial conditions but for different particle densities and inertia. Equation (4) is valid for small particle Stokes numbers ( $aU/\nu$ ) only. Therefore, our detailed study is restricted to  $St < 0.1$ ,  $A > 10$ .

In the *aerosol* ( $R < 2/3$ ) regime one expects that the particles exit the wake faster on average than the ideal tracers. The aerosol will be harder to be captured in the wake, since the centrifugal force along any closed orbit is pushing the particle outward. Figure 1 shows the inertial particle trajectories for increasing values of  $A$ . Certainly, the inertial trajectory has to converge to the passive one, as  $A$  increases, and this is indeed the case.

In the *bubble* ( $R > 2/3$ ) regime one expects that the par-

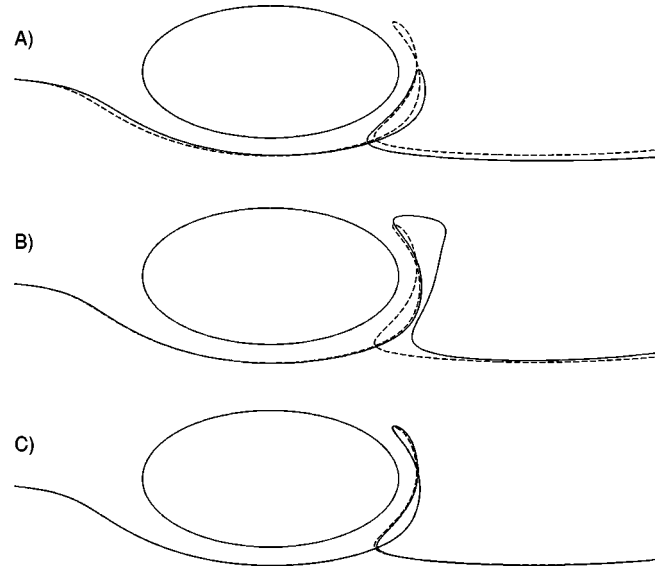


FIG. 1. Aerosol,  $R=0.5$ . Inertial and passive tracer trajectory comparison in the  $(x,y)$  plane. All trajectories were started from  $x_0 = -2.0$ ,  $y_0 = -0.11$  at  $t_0 = 0, w = 192/\pi$ . (A)  $A = 20$ , (B)  $A = 200$ , (C)  $A = 2000$ . The dashed line is the passive tracer's trajectory ( $A = \infty$ ).

ticle will be captured for longer times in the wake since the anticentrifugal force is an effective force of attraction towards the center of a closed orbit. In particular, the bubble will travel with the vortex for a longer period. As  $A$  increases the inertial trajectory converges to the passive one (Fig. 2).

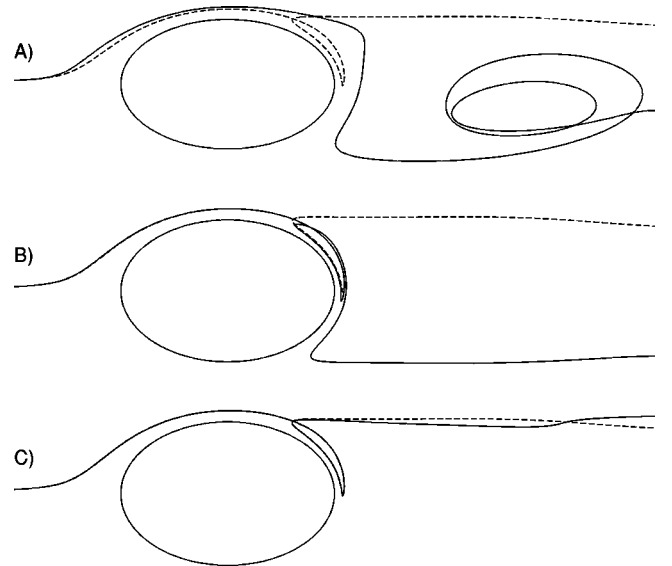


FIG. 2. Bubble,  $R=0.8$ . Inertial and passive tracer trajectory comparison. All trajectories were started from  $x_0 = -2.0$ ,  $y_0 = 0.06$  at  $t_0 = 0$ . All other parameters as in Fig. 1. The dashed line is the passive tracer's trajectory ( $A = \infty$ ). In all the runs, the particle's initial velocity is matched to that of the fluid.

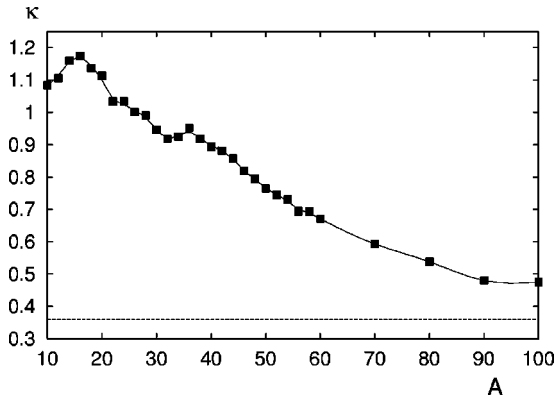


FIG. 3. Aerosol. Dependence of the escape rate on the inertia parameter  $A$  for  $R=0.5$ ,  $w=192/\pi$ . The horizontal line represents the Hamiltonian value of  $\kappa$ . We started  $10^6$  randomly distributed particles in the domain  $[0.6,4] \times [-2,2]$  around the cylinder and measured the number  $N(t)$  of surviving particles. A particle was considered to have escaped if it passed the line  $x=4$ , or if it approached the cylinder within a distance of 0.014. The exit on the surface of the cylinder was taken into account to separate the non-hyperbolic motion in the boundary layer from the dynamics in the wake. To determine  $\kappa$ , we took the average slope in the time period 2–9 of the  $\ln N$  vs  $t$  plot.

## V. ENSEMBLE DYNAMICS

### A. Escape rates

A statistical measure of the sensitive selectivity of the flow on the inertia and mass parameters is obtained from the study of the escape rate [25]. We start a large number of particles uniformly distributed in a fixed region in the wake. The number of nonescaped particles after time  $t$  is proportional to  $\exp(-\kappa t)$ , where  $\kappa$  is the escape rate.

The *passive advection* problem with  $w=192/\pi$  and  $w=24$  is characterized by the escape rate  $\kappa=0.36$  and  $\kappa=0.19$ , respectively.

From the *aerosol* regime we consider a fixed value of the mass ratio  $R$ , and study the escape rate as function of the inertia parameter  $A$ . One can observe (cf. Fig. 3) that the exponential decay of the aerosols takes place much faster than in the Hamiltonian case.

For the *bubble* regime we perform the same computation as in the case of aerosols. We find that the bubbles spend much more time in the wake. The escape rate vanishes in the range  $14 < A < 45$ , and then for  $A \rightarrow \infty$  it converges to the  $\kappa$  value obtained in the Hamiltonian case, as it should. This behavior is shown in Fig. 4. In the range  $14 < A < 45$  there is an extended region in the wake from which particles do not escape at all. Along with this, two isolated orbits behind the cylinder become attractive (for more detail concerning the attractors see Sec. VI). Both the efficient decrease of the escape rate and the disappearance of escape is interpreted as a statistical consequence of the anticentrifugal force acting on the bubbles [26], mentioned in Sec. IV.

### B. The residence time statistics

The region of vanishing  $\kappa$  in Fig. 4 implies that the inertia can modify the dynamics to the point where attractors appear

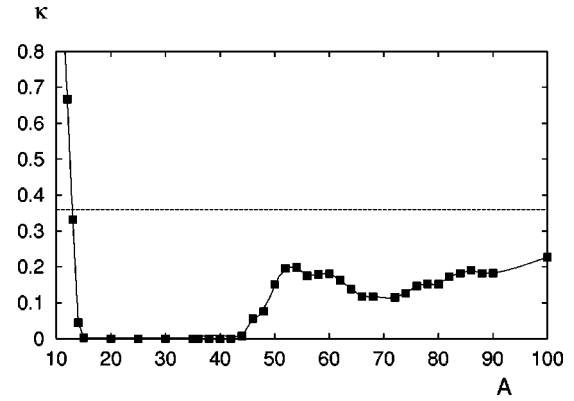


FIG. 4. Bubble. Dependence of the escape rate on the inertia parameter  $A$  for  $R=1.7$ ,  $w=192/\pi$ . The dashed line represents the Hamiltonian value of  $\kappa$ . We use the same  $10^6$  particle ensemble and perform the same steps as in the case of aerosols. We determine  $\kappa$  as the average slope in the time period 5–25 of the  $\ln N$  vs  $t$  plot. Error bars are in both Figs. 3 and 4 smaller than the size of the dots.

in the phase space with a visible component in the configuration space. In order to show this, in Fig. 5 we present the residence time [20] of the inertial tracers (in the bubble regime only) on the plane of initial conditions taken at a certain instant  $t_0$  of time (modulo the period  $T=1$  of the flow). The shades of blue, yellow and red depict residence times in increasing order. Dark red corresponds to initial conditions that lead to permanently trapped particles. The cylinder is shaded dark blue. By definition, the dark red domains correspond to the basin of attraction of the attractors that appeared in the configuration space.

As a comparison we include in Fig. 6 the residence times in the passive advection problem, too. The yellow filaments represent the stable manifold of the chaotic saddle that governs the passive dynamics. The red points correspond to small KAM tori appearing for this value of  $w$  in the advection dynamics (cf. the inset in Fig. 6).

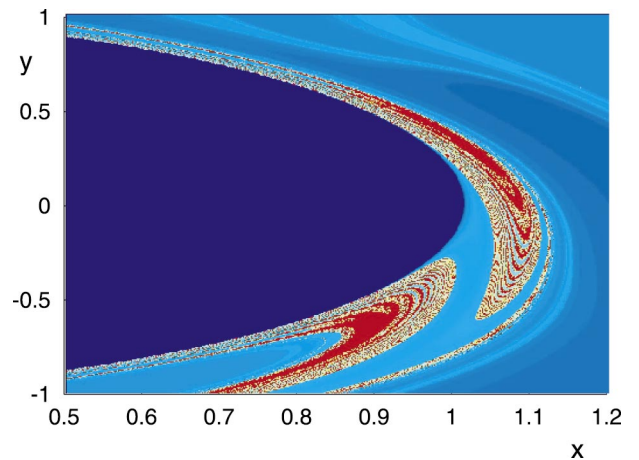


FIG. 5. (Color) Residence times for a bubble. The parameters are:  $A=30$ ,  $R=1.33$ ,  $w=24$ ,  $t_0=0.3$ . We started a particle in every point of a  $(540 \times 540)$  grid covering the region shown around the cylinder, and measured the time needed to leave this region downstream.

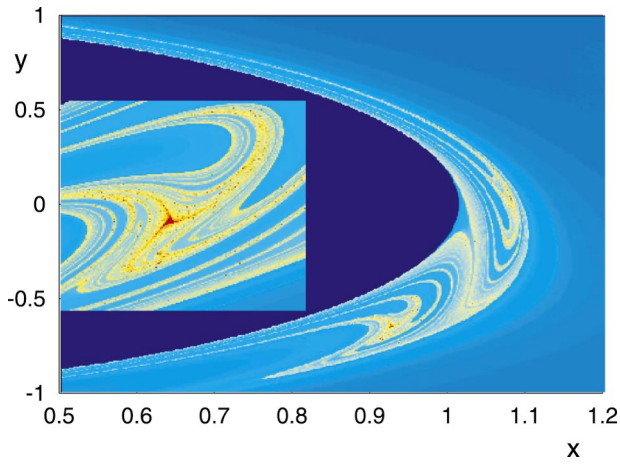


FIG. 6. (Color) Residence times for an ideal passive tracer. The parameters are:  $w=24$ ,  $t_0=0.3$ . The inset is a magnification of the domain  $[0.89, 0.94] \times [-0.75, -0.5]$ .

Due to inertia, these tori are transformed into attractors, and the basins of attraction appear along the stable filamentation of the Hamiltonian system. By changing the value  $w=24$  to  $w=192/\pi$  the tori of the Hamiltonian system disappear, and we find only purely hyperbolic orbits. Even in this case attractors can appear due to inertia [20]. Therefore, attractors can be formed from both marginally stable tori and purely unstable hyperbolic saddles of the passive advection's Hamiltonian dynamics.

### C. Different time scales in the decay dynamics

We recall that the passive advection problem of particle ensembles is characterized by an exponential decay only on short-time scales. This is caused by the existence of a chaotic saddle in the wake. In the long-time behavior, however, a power-law decay is observed due to the nearly marginally stable particle dynamics in the close vicinity of the surface of the cylinder [24].

In the inertial dynamics we observe—in contrast—two coexisting chaotic saddles in the wake (one on short and intermediate time scales) and a third nonhyperbolic chaotic set (on long-time scales), which is not only the obstacle's surface in this case. The short-time chaotic saddle is deformed in the limit  $A \rightarrow \infty$  into the saddle responsible to the chaotic behavior in the passive dynamics. The others have no direct counterparts in the passive advection problem, their presence being due to inertial effects.

The three different time scales associated with these invariant sets can be read off from the graph of the number of nonescaped particles vs time. In the log-lin plot one finds two segments with different slopes, the first in the range 0–5, the second in the range 6–25 time units, corresponding to the short- and intermediate-time scales [Fig. 7(a)], respectively. In the range of 30–150 time units the decay is different and tends towards a power law [Fig. 7(b)].

We present a detailed study at the fixed parameters:  $R=1.33$ ,  $A=30$ ,  $w=24$ , but emphasize that the behavior found here is typical. The classification of the decay dynamics holds in the whole  $A$  and  $R$  range where attractors exist.

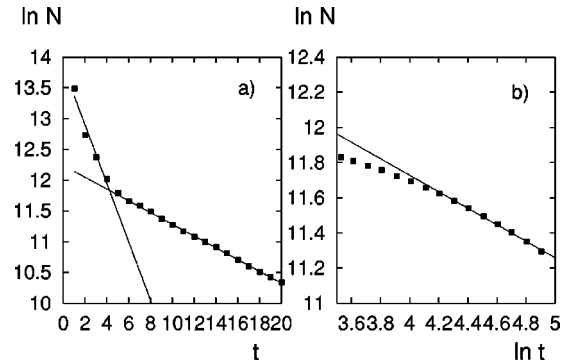


FIG. 7. The number of nonescaped particles vs time based on an ensemble initially covering the region  $[0.6, 4] \times [-2, 2]$ . (a) The log-lin plot shows two segments with different slopes. (b) The log-log plot shows a convergence towards a power law. To enhance this nonhyperbolic effect we did not cut out here the ring of width 0.014 around the cylinder [as we did in part (a)] which made the overall decrease of  $N$  slower. The parameters are  $R=1.33$ ,  $A=30$ ,  $w=24$ .

Note that in the aerosol range the escape is much faster and characterized by one single exponential decay. Hence the corresponding escape rate is extracted from the short time scales (see caption to Fig. 3).

In order to obtain the invariant sets, we used the method of Ref. [27]: the idea is based on choosing an appropriate number  $n$  of time units comparable with the average lifetime of chaos, and then following those particles from a large ensemble which do not escape the selected region of interest up to  $n$  time units. These survivors can only be those who came, within this period, sufficiently close to the chaotic saddle. Since such particles must have come in along the stable manifold and must leave the region along the unstable one, by plotting the positions of the surviving particles at times  $0, n/2$  and  $n$ , we obtain a good approximant to the saddle's stable manifold, to the saddle itself, and to its unstable manifold, respectively.

### D. Hyperbolic behavior

The *short-time* decay is due to a hyperbolic chaotic saddle, which is separating a direct escape downstream from a turning back towards the obstacle. The stable manifold of this saddle corresponds to the green filaments of Fig. 8. The points colored in magenta trace out the unstable manifold of this chaotic saddle. The chaotic saddle itself is the common part of the stable and unstable manifolds. The saddle is hyperbolic, which is manifest from its Cantor-set structure. It generates short, transiently chaotic trajectories, which exit the wake downstream.

The exponential decay *on intermediate time scales* is due to another chaotic saddle, which separates the escape to one of the two periodic attractors from the escape to the wall of the cylinder (Fig. 9). Since all the invariant sets lie in the full phase space, we show the saddle in the  $x, y, v_x$  space of the stroboscopic map. On this time scales we find particles that are trapped permanently in the wake. They have three possibilities: either to go directly to one of the attractors, or to first

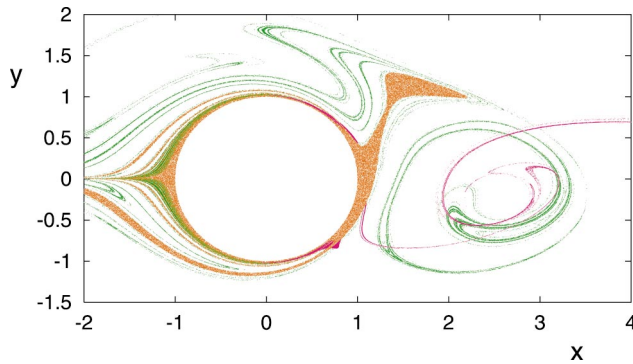


FIG. 8. (Color) Initial conditions of particles not leaving the region shown within the first time unit.  $R=1.33$ ,  $A=30$ ,  $w=24$ ,  $t_0=0$ . We started an ensemble initially covering the whole region shown, and measured the time needed to pass the line  $x=4$ . Points escaping within the first 4 units are colored green. The endpoint taken at time 4 of the particles trajectories starting from the green region is colored in magenta. Points in orange do not leave the wake over 100 time units.

approach the surface of the obstacle, then pass along the wall with velocity close to zero before being trapped by any of the attractors, permanently. Therefore, we can consider the wall as a temporary attractor. In order to determine this saddle and its manifolds, we determine a small region of linear size 0.014 around the attractors and around the cylinder, and consider a particle escaped if it falls within any of these regions.

The initial positions of the particles mentioned above lie in the *basin of attraction* of the attractors. The basins of attraction determined by this method [Fig. 10(a)] are of finite area and extend upstream (the orange domain of Fig. 8). This indicates that there is a nonzero probability for a randomly chosen particle to be trapped in the wake. By definition, the fractal boundary between the basins shown is the stable manifold of the chaotic saddle of Fig. 9.

To make the picture complete, we determined the unstable manifold of the saddle, too (see Fig. 11).

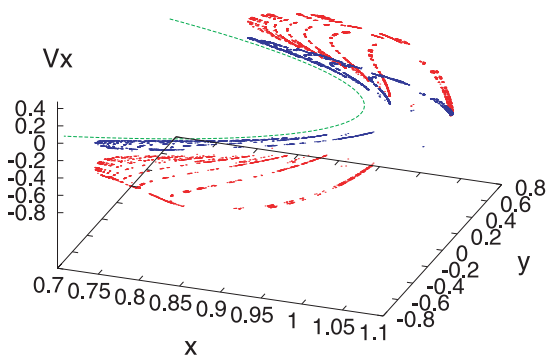


FIG. 9. (Color) The saddle (and its projection on the  $x, y$  plane—in blue) governing the dynamics on intermediate time scales  $5 < t < 20$  in 3D.  $R=1.33$ ,  $A=30$ ,  $w=24$ . The figure is obtained by plotting the positions at time 10 of the particles which started at time  $t=0$  and came close to the attractors between 20 and 25 time units. The green line represents the cylinder's surface.

## E. Nonhyperbolic behavior

On the long-time scales we find in the wake only those particles which came back from the boundary layer. Their behavior is dominated by nonhyperbolic effects. We have found that the saddle on this time scale is the same as the unstable manifold of Fig. 11. It does not exhibit any Cantor-set-like behavior in one direction of the plane of the flow. This local fattening up of the chaotic set is the reason of the power-law decay of the number of nonescaped particles [28–30].

In order to find the stable manifold of this chaotic set, we determine the basins of attraction in Fig. 10(b). The inter-spersion of the red and blue filaments is a sign of the basin's tendency to fill the 2D plane. Repeating the same measurements on longer-time scales (100 time units), the basin boundary, i.e., the stable manifold, appears to be two dimensional in the  $(x, y)$  plane. The boundary between the basins of attraction becomes a fat fractal, it fills the 2D plane, as a sign of nonhyperbolic behavior.

## VI. ATTRACTORS

As illustrated in Sec. V, our main observation is that in contrast to the passive case, bubbles *can get trapped permanently* in the wake of the obstacle. This means that due to inertia attractors appear in the phase space which are not present in the passive tracer limit.

A second important observation is that the longer lifetime of chaos and trapping is not only due to the surface of the cylinder. The attractors are actually situated in the wake, *away* from the boundary of the cylinder. The attractor at  $R=1.7$ ,  $A=30$ ,  $w=192/\pi$  is a period  $T=1$ , bean-shaped loop (on either sides of  $y=0$ ), i.e., it is a fixed point of the stroboscopic map. Figure 12 shows the form of one of these attractors, and the velocity-differences along the attractor.

A bounded particle trajectory can only exist if the particle is for some time faster, and then for some time slower than the flow. The inset of Fig. 12 shows the velocity of the particle and the relative velocity between particle and flow along a periodic attractor. Note that the integral of  $v_x - u_x$  is zero over one period.

As the particle becomes less dense, as  $R$  increases (at a fixed  $A$ ), these isolated periodic attractors are transformed into two chaotic attractors (Fig. 13) through an *inverse period-doubling sequence*, see Fig. 14. At smaller values of  $R$ , these chaotic attractors are transformed into a single attractor which contains the surface of the cylinder.

By fixing  $R=1.7$ , we obtain for both increasing and decreasing values of the size parameter  $A$  a period doubling bifurcation sequence (Fig. 15).

## VII. SEGREGATION

As a consequence of the results above, particles taken from a mixture of particles of different types have different dynamics as a function of size and inertia parameters. Therefore, segregation can take place, for example when we start with a mixture of particles of the same density but of different size (same  $R$ , different  $A$ ).

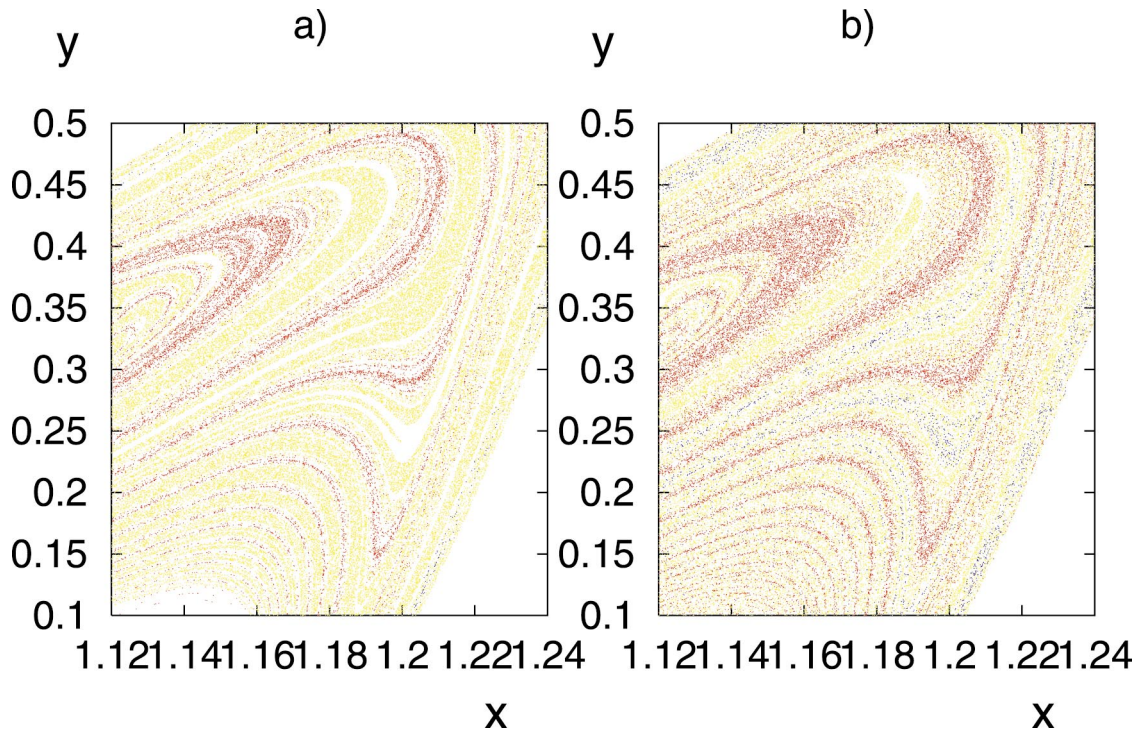


FIG. 10. (Color) Fractal boundary between the basins of attraction on intermediate time scales (a) and on long time scales (b). In (a) we plot the initial positions of the particles, which approached the cylinder within a distance of 0.014, or reached one of the two attractors in 20 time units. Points within the narrow white stripes have not yet reached any of the attractors by time 20. In (b) we plot the initial positions of the points which reach one of the attractors after 40 time units. The colors are: red/blue the basins of the upper/lower attractors and yellow the basin of attraction of the cylinder.  $R=1.33$ ,  $A=30$ ,  $w=24$ ,  $t_0=0$ .

Here we use a simple geometrical setup: the outgoing particle, which exits the chaotic region in the wake of an obstacle, becomes incoming particle for another obstacle, situated downstream from the first. We consider a chain of several cylinders [31] situated at a distance of 8 cylinder radius units from each other, where the flow field is approximately uniform. The fate of a droplet was followed which initially consisted of  $5 \times 10^4$  randomly distributed particles in the range  $[-2, -1.5] \times [-0.5, 0.5]$  with mass ratio  $R=1.4$  and with size:  $A=20$ ,  $A=120$ , colored in red and blue. After passing several cylinders, the droplet exhibits a separation of colors which is manifest from Fig. 16.

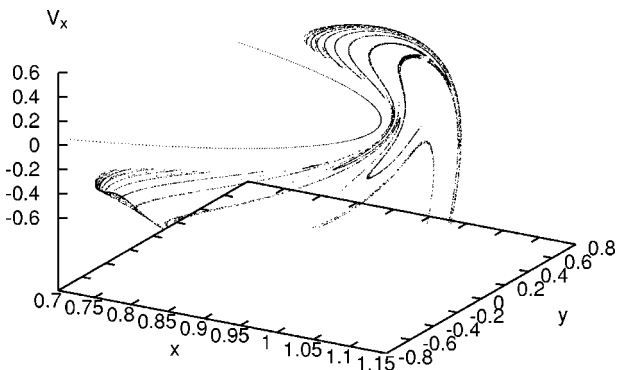


FIG. 11. The unstable manifold of the saddle on the intermediate time scales, obtained by plotting the endpoints at time 20 of the trajectories starting in the colored region of Fig. 10(a).

VIII. STABILIZING UNSTABLE ORBITS VIA INERTIA IN TIME PERIODIC FLOWS

A natural question to ask is how generic the phenomenon of trapping is, namely, if one can expect similar behavior in other types of flows as well. Our claim is that the phenomenon of trapping is a *generic* property resulting from the nonlinear interaction of the *temporal dependence* of the underlying flow and of the inertial effects. In order to show

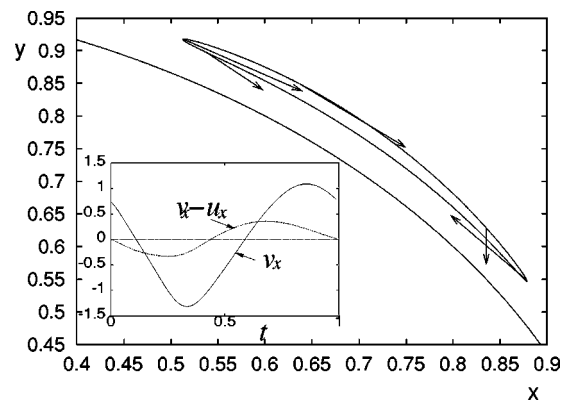


FIG. 12. The periodic attractor in the upper half plane, for  $R=1.7$ ,  $A=30$ ,  $w=192/\pi$ . We also show the relative velocity ( $\mathbf{v}-\mathbf{u}$ ) vectors (which determine the Stokes drag) along the attractor, at a few instants of time ( $t \in \{0.1, 0.5, 0.6, 0.8, 0.0\}$ ). The inset represents the velocity component  $v_x$  of the bubble and the relative velocity  $v_x - u_x$  between the tracer and the flow along the attractor.

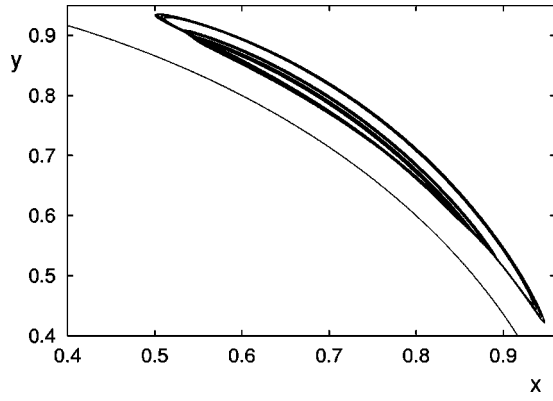


FIG. 13. The chaotic attractor in the upper half plane at  $R = 1.47$ ,  $A = 30$ ,  $w = 192/\pi$ .

this, we now present a proof-of-principle type of calculation in the case of a simple, generic flow model. This exhibits a single hyperbolic fixed-point in the origin (so a passive tracer would be repelled to infinity). We show that there is a parameter regime for *bubbles*, where this fixed-point becomes *attracting*. Let us consider for this purpose a two-dimensional flow which has the streamfunction [2]

$$\Psi(x, y, t) = \frac{G}{2}y^2 - \frac{GK}{2}x^2, \quad (12)$$

( $G$  and  $K$  are real). It generates the fluid velocity field  $\mathbf{u}$  with components  $u_x(x, y, t) = \partial\Psi/\partial y = Gy$  and  $u_y(x, y, t) = -\partial\Psi/\partial x = GKx$ . Therefore, the passive tracer motion is described by  $dx/dt = u_x(x, y, t) = Gy$ ,  $dy/dt = u_y(x, y, t) = GKx$ . It is easy to solve for the motion of the passive tracer in this flow field, provided  $G$  and  $K$  are constants [2].

When  $K > 0$ , the fixed point  $\mathbf{x} = \mathbf{0}$  is hyperbolic. The flow exponentially diverges to infinity along the direction of the eigenvector that belongs to the positive eigenvalue and, exponentially contracts in the direction along the other eigenvector. When  $K < 0$  the flow is purely rotational. For  $K = 0$  we have a pure shearing motion, see Fig. 17.

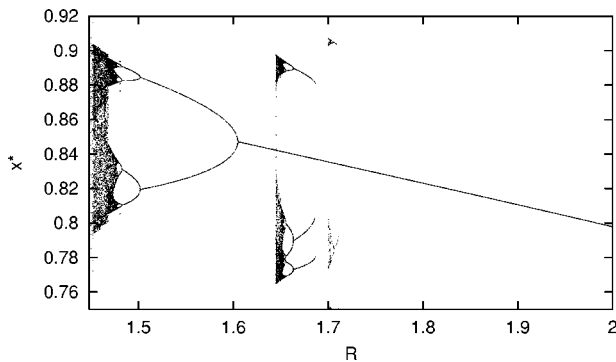


FIG. 14. The bifurcation diagram as a function of  $R$ . The parameters are:  $w = 192/\pi$ ,  $A = 30$ . The plot was obtained by starting 8000 particles in the range  $[0.5, 1.1] \times [-0.9, 0.9]$  of the wake and plotting their  $x$  coordinate after 520 time units.

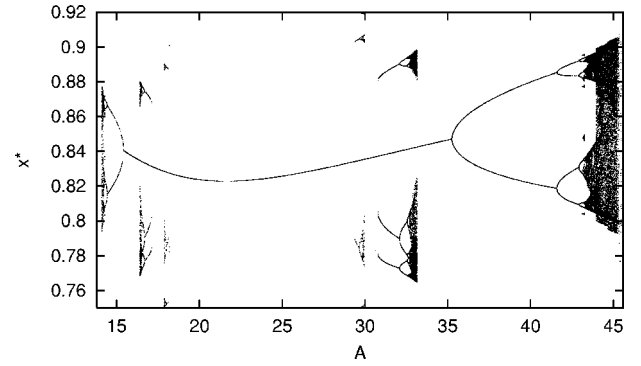


FIG. 15. The bifurcation diagram as a function of  $A$ . The parameters are:  $w = 192/\pi$ ,  $R = 1.7$ . The plot was obtained in an analogous way as Fig. 14.

### A. Inertial tracer motion

In the following we study how the inertia effects modify the tracer trajectory compared to the Hamiltonian motion of the ideal tracers. The full set of equations takes the form

$$\dot{x} = v_x, \quad (13)$$

$$\dot{y} = v_y, \quad (14)$$

$$\dot{v}_x = -Av_x + (3/2)RG^2Kx + AGy, \quad (15)$$

$$\dot{v}_y = -Av_y + AGKx + (3/2)RG^2Ky, \quad (16)$$

where dots represent time derivatives. By introducing the notations:  $Z_1 = x$ ,  $Z_2 = y$ ,  $Z_3 = v_x$ ,  $Z_4 = v_y$ ,  $\alpha = 3R/2$ , the system above becomes

$$\dot{\mathbf{Z}} = \mathbf{M}\mathbf{Z}, \quad (17)$$

where  $\mathbf{Z}$  is the  $4 \times 1$  column vector formed from  $Z_i$ ,  $i = 1, 2, 3, 4$ , and  $\mathbf{M}$  is the  $4 \times 4$  matrix:

$$\mathbf{M} = \begin{bmatrix} 0 & 0 & 1 & 0 \\ 0 & 0 & 0 & 1 \\ \alpha G^2 K & AG & -A & 0 \\ AGK & \alpha G^2 K & 0 & -A \end{bmatrix}. \quad (18)$$

Let

$$\begin{aligned} \Delta^{(\pm)} &= \sqrt{A^2 \pm 4AG\sqrt{K} + 4\alpha G^2 K} \\ &= \sqrt{(A \pm 2G\sqrt{K})^2 + 4(\alpha - 1)G^2 K} \end{aligned} \quad (19)$$

Then the four eigenvalues of  $\mathbf{M}$  are

$$\Lambda_1 = -\frac{A}{2} + \frac{\Delta^{(+)}}{2}, \quad \Lambda_2 = -\frac{A}{2} - \frac{\Delta^{(+)}}{2}, \quad (20)$$

$$\Lambda_3 = -\frac{A}{2} + \frac{\Delta^{(-)}}{2}, \quad \Lambda_4 = -\frac{A}{2} - \frac{\Delta^{(-)}}{2}. \quad (21)$$

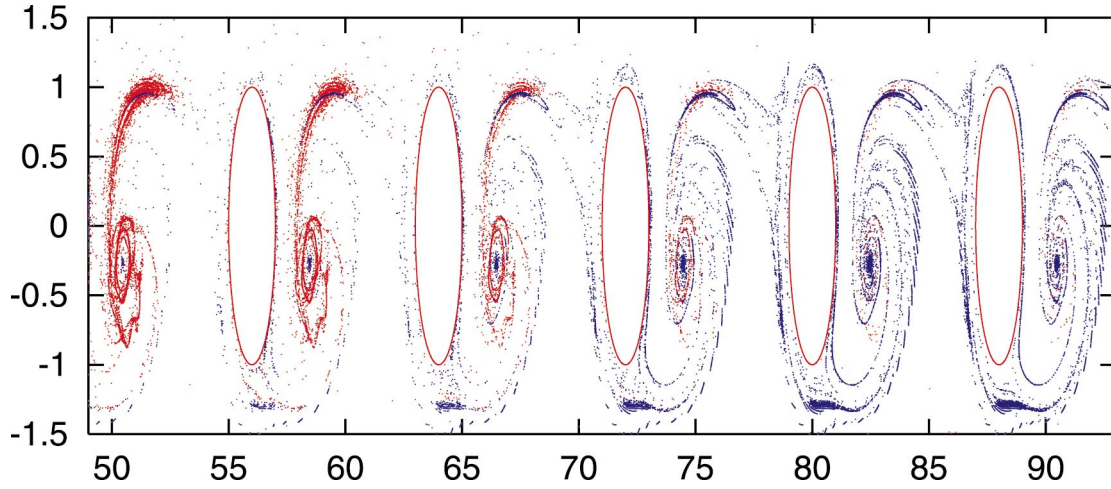


FIG. 16. (Color) A chaotic chromatograph: segregation of particles in the  $(x,y)$  plane after 10 time units in the periodic cylindrical flow with  $R=1.4$  and  $A=20$ ,  $A=120$ , colored in red and blue, respectively. Ellipses mark the cylinders.

**B. Time-periodic flow**

We redefine the streamfunction by replacing the constant  $G$  by the time-periodic form

$$G(t) = 1 + L \sin \omega t, \tag{22}$$

where  $L, \omega > 0$ .

**1. Hamiltonian tracer motion**

The passive tracer motion is described by

$$\dot{x} = u_x(x,y,t) = \frac{\partial \Psi}{\partial y} = G(t)y, \tag{23}$$

$$\dot{y} = u_y(x,y,t) = -\frac{\partial \Psi}{\partial x} = G(t)Kx. \tag{24}$$

It is easy to see from above that the Hamiltonian tracer trajectories in the  $(x,y)$  space remain the same as for the stationary ( $L=0$ ) case. The motion along these trajectories is changed however.

**2. Inertial tracer motion**

In this case, due to the explicit time-dependence, Eq. (4) retains the time derivatives of  $\mathbf{u}$  as well. We obtain

$$\dot{x} = v_x, \tag{25}$$

$$\dot{y} = v_y, \tag{26}$$

$$\dot{v}_x = -Av_x + \alpha G^2 Kx + (AG + \alpha \dot{G})y, \tag{27}$$

$$\dot{v}_y = -Av_y + (AG + \alpha \dot{G})Kx + \alpha G^2 Ky, \tag{28}$$

where  $\dot{G}(t) = L\omega \cos \omega t$ . The corresponding matrix equation is

$$\dot{\mathbf{Z}} = \mathbf{M}(t)\mathbf{Z}, \tag{29}$$

where

$$\mathbf{M}(t) = \begin{bmatrix} 0 & 0 & 1 & 0 \\ 0 & 0 & 0 & 1 \\ \alpha G^2 K & AG + \alpha \dot{G} & -A & 0 \\ (AG + \alpha \dot{G})K & \alpha G^2 K & 0 & -A \end{bmatrix}. \tag{30}$$

This system however is strongly nonautonomous which implies the difficulty of finding an exact solution. Instead of an exact solution, we are interested in showing that there can be values for the parameters such that the origin becomes an attractor for the inertial particle, in spite of the fact that for the Hamiltonian tracer the origin is a hyperbolic fixed point. Numerically, it is very easy

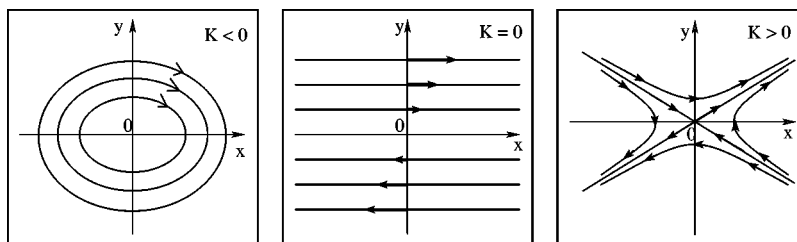


FIG. 17. Flow types for the model flow. Here  $G > 0$  was assumed.

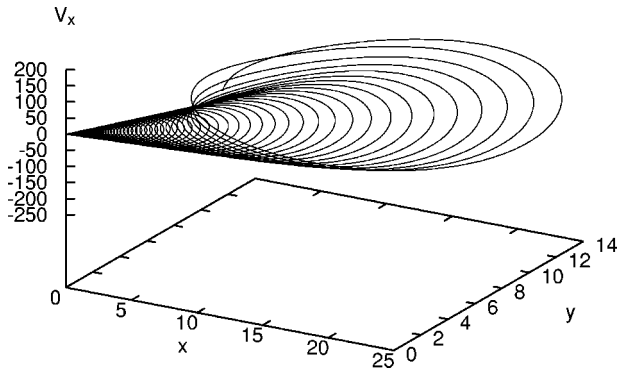


FIG. 18. Bubble trajectory spiraling into the origin for the time-periodic model. The parameters are:  $K=0.2$ ,  $A=20$ ,  $R=1.3$ ,  $\omega=6\pi$ ,  $L=15$ ,  $x_0=5.2$ ,  $y_0=6.5$ .

to find parameter values where the origin becomes attractive for  $K>0$ , see for example, Fig. 18.

We would like to find a condition for stabilizing the inertial particle to the origin when  $K>0$ . In order to further simplify the calculations, we assume that  $K=1$ . By introducing the variables

$$z(t)=x(t)+y(t), \quad v(t)=v_x(t)+v_y(t), \quad (31)$$

the equations of motion become

$$\dot{z}=v, \quad \dot{v}=-Av+a(t)z, \quad (32)$$

where

$$a(t)=\alpha G(t)^2+AG(t)+\alpha\dot{G}(t)=A+\alpha+L\alpha\omega\cos(\omega t)+L(A+2\alpha)\sin(\omega t)+L^2\alpha\sin^2(\omega t) \quad (33)$$

is a periodic function in time. The initial conditions must satisfy

$$v(t_0)=G(t_0)z(t_0). \quad (34)$$

The variable  $z(t)$  describes the projection of the motion on the first bisector. If the motion is bounded in the  $(x,y)$  coordinates, then the motion in  $z$  will be bounded, too. The converse is not necessarily true, and therefore requiring the stability of the origin in the  $z$  motion will be a necessary condition for the stability in the original motion. The system above is equivalent to the following second order differential equation:

$$\ddot{z}+A\dot{z}=a(t)z, \quad (35)$$

subject to initial conditions satisfying  $\dot{z}(t_0)=z(t_0)G(t_0)$ . After the transformation,  $u=\dot{z}/z+A/2$ , Eq. (35) becomes

$$\dot{u}+u^2=b(t) \quad (36)$$

with  $b(t)\equiv A^2/4+a(t)$ , and initial condition  $u(t_0)=G(t_0)+A/2$ . Thus, knowing a solution  $u(t)$ , one obtains a solution for  $z$  as

$$z(t)=z_0\exp\left\{-\frac{A}{2}(t-t_0)+\int_{t_0}^t u(s)ds\right\}. \quad (37)$$

This means that the asymptotic stability of the origin in  $z$  will be determined by the long-time behavior of the integral  $Q(t)=\int_{t_0}^t u(s)ds$ . If  $\bar{u}=\lim_{t\rightarrow\infty}Q(t)/t>A/2$  the origin is attracting, for  $\bar{u}=A/2$  it is marginally stable, and it is repelling, or unstable for  $\bar{u}<A/2$ .

## IX. CONCLUSIONS

Finite size and inertia effects may strongly modify the advection dynamics, in particular in the bubble regime. Here the escaping process becomes slower, attractors may appear, and if so, fractal boundaries are created between the basins of attractions. The attractors can be formed from both marginally stable tori and purely hyperbolic, unstable trajectories of the passive advection's Hamiltonian dynamics.

We have pointed out the possibility that by a proper engineering of the geometry of the open *chaotic* flow, selective inertial particle traps can be designed. The trapping phenomenon is at the same time a warning that a simple modeling of inertial particles as passive ideal tracers can lead to gross errors in forecasting particle motion. Our example shows that a harmful substance while modeled as a passive tracer will clear the wake of an obstacle, but in reality it may be indefinitely trapped there under the same conditions. These observations might explain the enhanced accumulation of pollutants in the atmospheric or aquatic media.

## ACKNOWLEDGMENTS

We are grateful to useful conversations with M. Chertkov, R. E. Ecke, G. Falkovich, M. Hastings, L. Margolin, and O. Piro. I. J. B. thanks S. Z. Benczik for discussions and encouragement. This effort was supported by the U.S. Department of Energy under Contract No. W-7405-ENG-36. The support of the Hungarian Science Foundation (OTKA, Grant No. T032423) and the MTA-OTKA-NSF Grant No. 526 are acknowledged.

- [1] H. Aref, *J. Fluid Mech.* **143**, 1 (1984).  
 [2] J.M. Ottino, *The Kinematics of Mixing: Stretching, Chaos, and Transport* (Cambridge University Press, Cambridge, 1989).  
 [3] S. Wiggins, *Chaotic Transport in Dynamical Systems* (Springer, New York, 1992).  
 [4] G. Segre and A. Silberberg, *Nature (London)* **189**, 209 (1961); *J. Fluid Mech.* **14**, 115 (1962).

- [5] M.R. Maxey and J.J. Riley, *Phys. Fluids* **26**, 883 (1983).  
 [6] M.R. Maxey, *Phys. Fluids* **30**, 1915 (1987).  
 [7] T.R. Auton *et al.*, *J. Fluid Mech.* **197**, 241 (1988).  
 [8] A. Crisanti *et al.*, *Phys. Fluids A* **4**, 1805 (1992).  
 [9] W.A. Sirignano, *ASME J. Fluids Eng.* **115**, 345 (1993).  
 [10] P. Tanga and A. Provenzale, *Physica D* **76**, 202 (1994).  
 [11] D.E. Stock, *ASME J. Fluids Eng.* **118**, 4 (1996).

- [12] T. Elperin, N. Kleeorin, and I. Rogachevskii, *Phys. Rev. Lett.* **77**, 5373 (1996).
- [13] E.E. Michaelides, *J. Fluids Eng.* **119**, 233 (1997).
- [14] A. Bracco *et al.*, *Phys. Fluids* **11**, 2280 (1999).
- [15] A. Babiano *et al.*, *Phys. Rev. Lett.* **84**, 5764 (2000).
- [16] E. Balkovsky, G. Falkovich, and A. Fouxon, *Phys. Rev. Lett.* **86**, 2790 (2001).
- [17] T. Shinbrot *et al.*, *Phys. Rev. Lett.* **86**, 1207 (2001).
- [18] R. Reigada, F. Sagues, and J.M. Sancho, *Phys. Rev. E* **64**, 026307 (2001).
- [19] C. Lopez, *Phys. Rev. E* **66**, 027202 (2002).
- [20] I. J. Benczik, Z. Toroczkai, and T. Tél, *Phys. Rev. Lett.* **89**, 164501 (2002).
- [21] J.H.E. Cartwright, M.O. Magnasco, and O. Piro, *Phys. Rev. E* **65**, 045203 (2002); *Chaos* **12**, 489 (2002).
- [22] T. Nishikawa, Z. Toroczkai, and C. Grebogi, *Phys. Rev. Lett.* **87**, 038301 (2001); T. Nishikawa, Z. Toroczkai, C. Grebogi, and T. Tél, *Phys. Rev. E* **65**, 026216 (2002).
- [23] I.M. Jánosi *et al.*, *Phys. Rev. E* **56**, 2858 (1997).
- [24] C. Jung, T. Tél, and E. Ziemniak, *Chaos* **3**, 555 (1993).
- [25] T. Tél, in *Directions in Chaos*, edited by Hao Bai-Lin (World Scientific, Singapore, 1990), Vol. 3, p. 149.
- [26] G. Falkovich, A. Fouxon, and M.G. Stepanov, *Nature (London)* **419**, 151 (2002); M.R. Maxey, *J. Fluid Mech.* **226**, 1 (1987).
- [27] Y.-C. Lai, T. Tél, and C. Grebogi, *Phys. Rev. E* **48**, 709 (1993).
- [28] Y.-T. Lau, J.M. Finn, and E. Ott, *Phys. Rev. Lett.* **66**, 978 (1991).
- [29] F. Christiansen and P. Grassberger, *Phys. Lett. A* **181**, 47 (1993).
- [30] A.E. Motter and Y.-C. Lai, *Phys. Rev. E* **65**, 015205(R) (2002).
- [31] M.A. Sanjuan *et al.*, *Phys. Rev. Lett.* **78**, 1892 (1997); *Chaos* **7**, 125 (1997).